ORIGINAL PAPER

Increased pyroptosis activation in white matter microglia is associated with neuronal loss in ALS motor cortex

Evelien Van Schoor[1,2,3] · Simona Ospitalieri[1] · Sebastiaan Moonen[1,3,4] · Sandra O. Tomé[1] · Alicja Ronisz[1] · Orkun Ok[1] · Jochen Weishaupt[5,6] · Albert C. Ludolph[5,7] · Philip Van Damme[2,3,8] · Ludo Van Den Bosch[2,3] · Dietmar Rudolf Thal[1,9]

Abstract

Amyotrophic lateral sclerosis (ALS) is characterized by the degeneration of motor neurons in the motor cortex, brainstem, and spinal cord. Although ALS is considered a motor neuron disorder, neuroinflammation also plays an important role. Recent evidence in ALS disease models indicates activation of the inflammasome and subsequent initiation of pyroptosis, an inflammatory type of cell death. In this study, we determined the expression and distribution of the inflammasome and pyroptosis effector proteins in *post-mortem* brain and spinal cord from ALS patients ($n = 25$) and controls ($n = 19$), as well as in symptomatic and asymptomatic TDP-43[A315T] transgenic and wild-type mice. Furthermore, we evaluated its correlation with the presence of TDP-43 pathological proteins and neuronal loss. Expression of the NOD-, LRR-, and pyrin domain-containing protein 3 (NLRP3) inflammasome, pyroptosis effector protein cleaved Gasdermin D (GSDMD), and IL-18 was detected in microglia in human ALS motor cortex and spinal cord, indicative of canonical inflammasome-triggered pyroptosis activation. The number of cleaved GSDMD-positive precentral white matter microglia was increased compared to controls and correlated with a decreased neuronal density in human ALS motor cortex. Neither of this was observed in the spinal cord. Similar results were obtained in TDP-43[A315T] mice, where microglial pyroptosis activation was significantly increased in the motor cortex upon symptom onset, and correlated with neuronal loss. There was no significant correlation with the presence of TDP-43 pathological proteins both in human and mouse tissue. Our findings emphasize the importance of microglial NLRP3 inflammasome-mediated pyroptosis activation for neuronal degeneration in ALS and pave the way for new therapeutic strategies counteracting motor neuron degeneration in ALS by inhibiting microglial inflammasome/pyroptosis activation.

Keywords Amyotrophic lateral sclerosis · Inflammasome · Pyroptosis · Transactive response DNA-binding protein

✉ Evelien Van Schoor
   evelien.vanschoor@kuleuven.be

✉ Dietmar Rudolf Thal
   dietmar.thal@kuleuven.be

1 Laboratory of Neuropathology, Department of Imaging and Pathology, KU Leuven (University of Leuven), Leuven Brain Institute (LBI), O&N IV Herestraat 49-bus 1032, 3000 Leuven, Belgium

2 Laboratory of Neurobiology, Department of Neurosciences, KU Leuven (University of Leuven), Leuven Brain Institute (LBI), Leuven, Belgium

3 Center for Brain & Disease Research, VIB, Leuven, Belgium

4 Laboratory for the Research of Neurodegenerative Diseases, Department of Neurosciences, KU Leuven (University of Leuven), Leuven Brain Institute (LBI), Leuven, Belgium

5 Department of Neurology, Ulm University, Ulm, Germany

6 Divisions of Neurodegeneration, Department of Neurology, Mannheim Center for Translational Neurosciences, Medical Faculty Mannheim, Heidelberg University, Mannheim, Germany

7 Deutsches Zentrum für Neurodegenerative Erkrankungen, Ulm, Germany

8 Department of Neurology, University Hospitals Leuven, Leuven, Belgium

9 Department of Pathology, University Hospitals Leuven, Leuven, Belgium

Abbreviations

ALRs	Absent in melanoma-like receptors
ALS	Amyotrophic lateral sclerosis
ASC	Apoptosis-associated speck-like protein containing a CARD
ATP	Adenosine triphosphate
Aβ	Amyloid beta
C9ORF72	Chromosome 9 open-reading frame 72
CARD	Caspase recruitment domain
CERAD	Consortium to Establish a Registry for Alzheimer's disease
CNS	Central nervous system
DAMPs	Damage-associated molecular patterns
DAB	3,3′-Diaminobenzidine
FTLD	Frontotemporal lobar degeneration
FTD	Frontotemporal dementia
FTLD-TDP	Frontotemporal lobar degeneration with TDP-43 pathology
GAPDH	Glyceraldehyde-3-phosphate dehydrogenase
GSDMD	Gasdermin D
GSDMD-NT	Gasdermin D N-terminal region
HRP	Horseradish peroxidase
IL	Interleukin
IHC	Immunohistochemistry
MTL	Medial temporal lobe
NFT	Neurofibrillary tangle
NFκB	Nuclear factor-κB
NLRs	Nucleotide-binding domain and leucine-rich repeat-containing receptors
NLRP3	NOD-, LRR-, and pyrin domain-containing protein 3
PAMPs	Pathogen-associated molecular patterns
PRP	Prion protein
PRRs	Pattern recognition receptors
pTDP-43	Phosphorylated transactive response DNA-binding protein 43 kDa
PYD	Pyrin domain
ROS	Reactive oxygen species
SDS-PAGE	Sodium dodecyl sulfate-polyacrylamide gel electrophoresis
SOD1	Superoxide dismutase-1
TBS	Tris-buffered saline
TDP-43	Transactive response DNA-binding protein 43 kDa
TLRs	Toll-like receptors

Introduction

Amyotrophic lateral sclerosis (ALS) is a neurodegenerative disorder characterized by progressive muscular paralysis resulting from degeneration of both the upper motor neurons situated in the primary motor cortex, and the lower motor neurons situated in the brainstem and spinal cord [17]. This rare disease affects 1–3 individuals per 100,000 per year [37, 41]. ALS patients usually die due to respiratory failure within 2–5 years following disease onset [49]. In approximately 10% of ALS cases, there is a family history of the disease (familial ALS), whereas for most of the sporadic ALS cases, the cause is unknown [36]. The main pathological characteristic of 97% of ALS patients is the cytoplasmic mislocalization and aggregation of transactive response DNA-binding protein 43kD (TDP-43) in affected central nervous system (CNS) regions [33]. TDP-43 inclusions are also found in about 50% of patients with frontotemporal lobar degeneration (FTLD), referred to as FTLD-TDP [13]. It has become clear that ALS and FTLD belong to a disease spectrum as up to 50% of ALS patients show some features of FTLD and hexanucleotide repeat expansions in the *C9orf72* gene are the most common genetic cause of ALS and FTLD [40]. Although ALS is considered a motor neuron disorder, non-cell autonomous mechanisms, such as neuroinflammation, are believed to significantly contribute to ALS pathogenesis. This suggests that glial cells also contribute to motor neuron degeneration observed in the ALS CNS [27, 34].

Inflammasomes were shown to play an important role in neuroinflammation and neurodegeneration. These are multiprotein complexes mainly located in immune cells, neurons, microglial cells, and astrocytes in the CNS [15]. They function as cytosolic scaffolds assembled by pattern recognition receptors (PRRs), and are responsible for detecting and eliminating pathogen-associated molecular patterns (PAMPs) and damage-associated molecular patterns (DAMPs). The sensors of the inflammasome can be classified into three types, including nucleotide-binding domain and leucine-rich repeat-containing receptors (NLRs), absent in melanoma-like receptors (ALRs) and pyrin. The adaptor protein apoptosis-associated speck-like protein containing a CARD (ASC) links the pyrin domain (PYD) of these sensors to the caspase recruitment domain (CARD) of pro-caspase-1. However, some inflammasomes can directly recruit pro-caspase-1, without the adaptor protein ASC [46]. The assembly and activation of the inflammasome is cell type and stimulus specific. The most investigated sensor protein is NLRP3, which is thought to be the main sensor for sterile inflammatory stimuli, while for example NLRC4 mainly acts as a sensor of bacterial infection [9, 15, 50].

The activation of the inflammasome through the canonical signaling pathway causes cleavage of pro-caspase-1 into active caspase-1 fragments (caspase-1 p20). Subsequently, caspase-1 cleaves biologically inactive pro-IL-1β and pro-IL-18 into the mature inflammatory cytokines IL-1β and IL-18. In addition, caspase-1 cleaves and activates Gasdermin D (GSDMD) leading to the release of an N-terminal

region (GSDMD-NT), which oligomerizes and binds to acidic phospholipids, such as phosphoinositides on the inner part of the plasma membrane, to form death-inducing pores. This causes cell swelling, rupture of the plasma membrane, and the release of IL-1β and IL-18 to the extracellular space, inducing the pro-inflammatory type of regulated cell death known as pyroptosis. It is thought that cleaved GSDMD, which functions as the effector of pyroptosis, might target and perforate multiple organelles, in addition to the plasma membrane [12, 15]. Extracellular IL-18 and IL-1β can also recruit and activate other immune cells, expanding the local inflammatory response. In the CNS, microglial cells, astrocytes, and neurons can all undergo pyroptosis and express its related downstream molecules and receptors, taking part in the local inflammatory reaction [50].

The NLRP3 inflammasome has been implicated in several neurodegenerative disorders, as it was shown that the inflammasome could be activated by abnormal protein aggregation, including for example amyloid-β in Alzheimer's disease [19] and α-synuclein in Parkinson's disease [47]. For ALS, most research related to the inflammasome and pyroptotic cell death has been conducted in mutant superoxide dismutase-1 (SOD1) animal models. Multiple studies showed an upregulation of the expression of several NLRP3 inflammasome components, as well as the cytokines IL-18 and IL-1β, in the CNS of SOD1 mice and rats compared to controls [2, 8, 16, 22]. Moreover, it was demonstrated that mutant SOD1 could activate microglial cells, leading to caspase-1 activation and consequent cleavage of IL-1β. This was not the case when microglial cells were deficient for NLRP3, suggesting that NLRP3 is the key inflammasome in mediating SOD1-induced microglial pyroptosis activation [10, 29]. For TDP-43, there is evidence that mutant and aggregated forms of TDP-43 can trigger NLRP3 inflammasome-dependent IL-1β and IL-18 secretion in vitro in microglia, which was toxic to motor neurons [25, 53]. In the absence of microglia, TDP-43 was not toxic to motor neurons [53]. Whether this NLRP3 inflammasome-related microglia activation as observed in mouse models and in vitro aggregation models plays a role in sporadic ALS patients, and whether this is related to TDP-43 pathology and neuronal degeneration, remains unclear.

Materials and methods

Human autopsy cases

Brain and spinal cord tissue was collected in accordance with the applicable laws in Belgium (UZ Leuven) and Germany (Ulm). The recruitment protocols for collecting the brains were approved by the ethical committees of the University of Ulm (Germany) and UZ Leuven (Belgium). This study was approved by the UZ Leuven ethical committee (Belgium).

Tissues were collected with an average *post-mortem* interval of 44 h. After autopsy, the right hemisphere was dissected in coronal planes and frozen at − 80 °C. The left hemisphere was fixed in 4% phosphate-buffered formaldehyde. 25 ALS cases (15 sporadic and 10 *C9orf72*) and 19 non-neurodegenerative controls were included in this study (Suppl. Table 1, online resource). The diagnosis of ALS or FTD was based on clinical assessment according to the consensus criteria for ALS [4–6] and FTD [14, 35]. The *post-mortem* diagnosis of ALS and FTLD-TDP was pathologically confirmed by assessment of the pTDP-43 pathology. Braak NFT stage [3], AβMTL phase [42], and the Consortium to Establish a Registry for Alzheimer's disease (CERAD) score [31] were determined based on immunohistochemical stainings with antibodies against Aβ and abnormally phosphorylated tau protein (p-tau) (Suppl. Table 2, online resource).

C9orf72 repeat expansion determination

DNA was extracted from peripheral blood and/or cerebellum according to standard protocols. Analysis of the hexanucleotide repeat length in intron 1 of *C9orf72* was performed by fragment length analysis by PCR and repeat-primed PCR (RP-PCR) as previously described [7]. In addition, the presence of poly(GA) pathology was immunohistochemically assessed in the frontal cortex. The *C9orf72* mutation status is shown in Suppl. Table 1 (online resource).

Transgenic mice

Heterozygous mice overexpressing a TDP-43 construct containing the A315T mutation driven by the mouse prion protein (Prp) promotor (Prp-hTDP-43^{A315T}) were used in this study [48]. Transgenic mice were bred by continuous backcrossing of heterozygous males with wild-type females on a C57BL/6 background. Due to intestinal obstruction problems in this model, the animals were given gel food from the age of two months onwards (DietGel®31 M, ClearH2O, Portland, ME, US), which is known to overcome this problem [20]. Five groups of mice (total $n = 28$) were used: (1) wild-type non-transgenic mice at 6 months of age ($n = 3$), (2) Prp-hTDP-43^{A315T} mice at 6 months of age ($n = 4$), (3) non-transgenic mice at 16 months of age ($n = 4$), (4) Prp-hTDP-43^{A315T} mice at 16 months of age ($n = 7$), and (5) symptomatic Prp-hTDP-43^{A315T} mice ($n = 5$; 6–14 months of age, mean age of 9 months). In group 5, mice were sacrificed 1–3 days following symptom onset, i.e., detection of impaired and reduced movement in the cage. Mouse brains and spinal cords were harvested after death and fixed in 4% paraformaldehyde for 3–5 days. After paraffin embedding, sections of 5 μm were cut with a microtome and used for immunohistochemistry. All animal care and experiments

were approved by the KU Leuven Ethical Committee and were carried out according to the Belgian law.

Immunohistochemistry

Human samples

Five-µm-thick sections were cut from formalin-fixed, paraffin-embedded tissue of motor cortex and spinal cord. Sections were stained with antibodies against pTDP-43, Aβ, p-tau, cleaved GSDMD, caspase-1, IL-18, ASC, and NLRP3 (Suppl. Table 2, online resource). Stainings were performed with the BOND-MAX automated IHC/ISH Stainer (Leica Biosystems, Wetzlar, Germany) using the Bond Polymer Refine Detection kit (DS9800, Leica Biosystems). Briefly, slides were deparaffinized and epitopes were retrieved with low or high pH buffer. After incubation with Envision Flex Peroxidase-Blocking Reagent (Dako, Glostrup, Denmark), slides were incubated with primary antibodies for 30 min, followed by secondary antibody incubation. DAB was used for visualization. Counterstaining with hematoxylin was carried out, followed by dehydration and mounting in an automated cover-slipper (Leica Biosystems). Images were acquired using the Leica DM2000 LED microscope coupled to a Leica DFC 7000 T camera. Images were processed using ImageJ and combined into figures using Inkscape.

For immunofluorescence double labeling using primary antibodies from different species (Suppl. Table 2, online resource), an antibody cocktail of the respective primary antibodies was applied, followed by a cocktail of species-specific Cy2/3-conjugated secondary antibodies (Jackson ImmunoResearch, Ltd, West Grove, PA, USA). For double labeling with primary antibodies raised in the same species (Suppl. Table 2, online resource), a sequential staining was performed using a rabbit-on-rabbit staining protocol as previously described [45]. Briefly, a coupling method was used to avoid cross-reactivity of secondary antibodies. The first rabbit primary antibody was used as described above, followed by a Cy2-labeled donkey anti-rabbit secondary antibody. The second rabbit primary antibody was coupled to a donkey anti-rabbit Fab fragment conjugated to a Cy3 dye for 20 min (2 µg Fab fragment per 1 µg primary antibody) prior to its incubation with the sample. Next, normal rabbit serum (Jackson ImmunoResearch) was added for another 10 min to capture the unbound Fab fragments (10 µl serum per 1 µg Fab fragment). Then, the mix was applied to the slides to visualize the second primary antibody. TrueBlack Lipofuscin Autofluorescence Quencher (Biotum, CA, USA) was applied for 30 s to reduce autofluorescence. Fluorescent-labeled slides were mounted using

ProLong Gold Antifade Mountant containing DAPI (Thermo Fisher Scientific, Rockford, IL, USA) for counterstaining of the nuclei. Images were acquired with a Leica SP8X confocal microscope (Leica Microsystems, Wetzlar, Germany) at a magnification of $63\times$ using type F immersion oil (Leica Microsystems). Images were processed using ImageJ and combined into figures using Inkscape.

Mouse samples

Mouse brain sections were stained with antibodies against TDP-43, ubiquitin, GSDMD, caspase-1, p62 and Iba1 (Suppl. Table 2, online resource). Stainings were performed manually, similar to immunohistochemistry and immunofluorescence of the human slides. An extra mouse IgG blocking step was performed to prevent unspecific signal. For GSDMD, proteinase K treatment was additionally applied for 1 min.

pTDP-43 pathology and TDP-43 nuclear clearance quantification in human samples

pTDP-43 pathology was assessed in the motor cortex and the anterior horn of the lumbosacral spinal cord of human cases. The amount of pathological inclusions in a $20\times$ microscopic field with most abundant pathology, considered as the "hotspot area", was quantified. The abundance of pathology was expressed as a percentage of neurons affected by pTDP-43 pathology. For quantification of the percentage of neurons with TDP-43 cleared form the nucleus in layer V of the motor cortex, two images (0.632×0.474 mm) of anti-TDP-43 (C-terminal) stained sections were taken using a $20\times$ objective. Image J was used for quantifications. The percentage of neurons without TDP-43 in the nucleus was calculated in relation to all neurons present in the respective region of interest.

TDP-43 nuclear clearance quantification in mouse samples

For quantification of the percentage of neurons with TDP-43 cleared from the nucleus in the motor cortex and anterior horn of the spinal cord of all mice, two images (0.632×0.474 mm) of anti-TDP-43 (C-terminal) stained sections were taken with the Leica DM2000 LED microscope using a $20\times$ objective. Image analysis was performed using ImageJ. The percentage of neurons without TDP-43 in the nucleus was calculated in relation to all neurons present in the respective region of interest.

Quantification of number of cleaved GSDMD- and caspase-1-positive glia/neurons

Human samples

For quantification of the number of cleaved GSDMD- and caspase-1-positive microglial cells and neurons in the precentral white matter and in layer V of the motor cortex, three consecutive images (0.632 × 0.474 mm) of anti-cleaved GSDMD- and anti-caspase-1-stained sections were taken with the Leica DM2000 LED microscope using a 20 × objective. For the lumbar spinal cord ventral pyramidal tracts, one 20 × image was acquired, while for the lateral pyramidal tracts two 20 × images were used. For the lumbar spinal cord anterior horn, two 10 × images (1.264 × 0.948 mm) were used. Microglial cells were identified by their shape and nuclear morphology. Image analysis was performed using ImageJ.

Mouse samples

For quantification of the number of microglial cells positive for GSDMD and caspase-1 per mm^2 in the motor cortex (gray and white matter) and spinal cord (anterior horn and pyramidal tracts) of all mice, four images (0.632 × 0.474 mm) of anti-GSDMD- and anti-caspase-1-stained sections were taken with the Leica DM2000 LED microscope using a 20 × objective. Microglial cells were identified by their shape and nuclear morphology. Image analysis was performed using ImageJ.

Quantification of neuronal density in the motor cortex and spinal cord

Human samples

For quantification of neuronal density in layer V of the motor cortex, three consecutive images (0.632 × 0.474 mm) of a representative area of anti-cleaved GSDMD-stained sections were taken with the Leica DM2000 LED microscope using a 20 × objective [24]. For quantification of neuronal density in the anterior horn of the lumbosacral spinal cord, two images (1.264 × 0.948 mm) of a representative area of anti-cleaved GSDMD-stained sections were taken using a 10 × objective. Criteria regarding morphological conditions of neurons to be included were determined before quantification. Neurons were identified based on their nuclear pattern in the hematoxylin staining. Image analysis was performed using ImageJ.

Mouse samples

For quantification of neuronal density in layer V of the motor cortex and in the anterior horn of the spinal cord, two images (0.632 × 0.474 mm) of anti-TDP-43-stained sections were taken with the Leica DM2000 LED microscope using a 20 × objective. Criteria regarding morphological conditions of neurons to be included were determined before quantification, similar as for the human samples. Image analysis was performed using ImageJ.

Protein extraction

For biochemistry, the spinal cord was taken and the right brain hemisphere was cut in approx. 1 cm-thick slabs and frozen at – 80 °C. Fifty mg of brain or spinal cord tissue was weighed and mechanically homogenized in 0.5 ml 2% SDS in TBS (Tris-buffered saline) with Nuclease (Pierce™ Universal Nuclease, Thermo Fisher Scientific) and a cocktail of protease/phosphatase inhibitors (Halt, Thermo Fisher Scientific) using a micropestle. Samples were sonicated, followed by a centrifugation at 14,000 *g* for 30 min. The resulting supernatant was used. Protein concentrations were determined using the Pierce BCA Protein Assay Kit (Thermo Fisher Scientific).

Western blotting

For western blotting, 10 µg of protein was loaded on a Bis–Tris 4–12% gradient SDS-PAGE (Invitrogen, Thermo Fisher Scientific) in MOPS/MES-SDS running buffer (Alfa Aesar, Haverhill, MA, USA), electrophoresed at 150 V for 60 min, and transferred to a nitrocellulose membrane (Semidry transfer, Biorad, Hercules, CA, USA). Membranes were blocked with 5% non-fat dried milk (AppliChem, Darmstadt, Germany) in PBS 0.1% Tween-20 (PBST). Primary antibodies and the corresponding dilutions are listed in Suppl. Table 2 (online resource). Secondary antibodies were goat anti-rabbit IgG-HRP or goat anti-mouse IgG-HRP (1:10 000, polyclonal, Dako). Blots were developed with SuperSignal West Pico or Dura plus ECL reagent (Thermo Fisher Scientific). Digital images were acquired using the Amersham Imager 600 (GE Healthcare, Chicago, IL, USA). All blots were stripped (Restore Western Blot Stripping Buffer, Thermo Fisher Scientific) of bound antibodies and reprobed with GAPDH to control for equal protein loading. Band intensities were measured using ImageJ and were normalized to GAPDH.

Statistical analysis

Statistical analyses were performed using IBM SPSS and Graphpad Prism software. Binary logistic regression
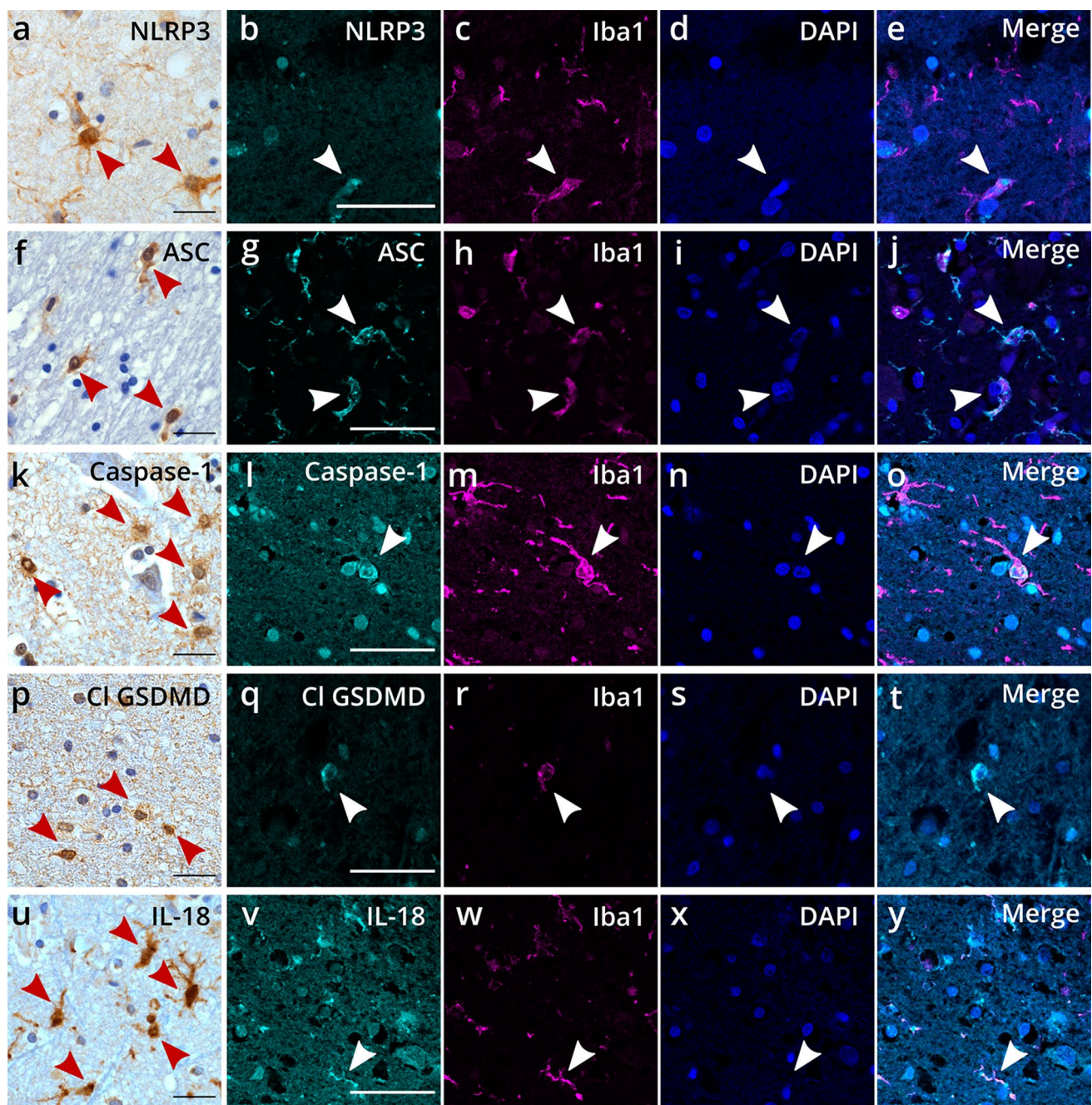
Fig. 1 Expression of inflammasome components and pyroptosis effector-related proteins in ALS precentral white matter microglia. Immunohistochemical and immunofluorescence detection of inflammasome components NLRP3 (**a–e**), ASC (**f–j**), and caspase-1 (**k–o**), as well as pyroptosis effector-related proteins cleaved GSDMD (**p–t**) and IL-18 (**u–y**) in representative ALS precentral white matter. Arrowheads indicate microglial cells positive for the respective markers. Scale bars represent 50 µm

controlled for age and sex, or a *t* test or Mann–Whitney test were used to determine the significant difference between two groups. To examine the different mouse groups, a one-way ANOVA or Kruskal–Wallis test was used followed by a post hoc test to correct for multiple testing. To examine correlations between motor cortex layer V neuronal density or anterior horn spinal cord neuronal density and several parameters, partial Pearson's correlation analysis (controlled for age and sex for the human cohort) was performed. To estimate the effect of explanatory variables on human motor cortex layer V neuronal density, we conducted linear regression analyses. Data are presented as mean $\pm$ SEM. $*p < 0.05$; $**p < 0.01$; $***p < 0.001$; $****p < 0.0001$.

Results

The canonical NLRP3 inflammasome as well as pyroptosis effector-related proteins are expressed in microglial cells in the ALS motor cortex

To investigate the expression of NLRP3 inflammasome components in the ALS brain, we performed a pathological analysis on human *post-mortem* brain tissue from ALS ($n = 24$) and control ($n = 12$) cases (Suppl. Table 1, online resource). For this, we used motor cortex, as this is the main affected brain region in ALS. Immunohistochemical staining showed positive immunoreactivity for NLRP3 (Fig. 1a), ASC (Fig. 1f), and caspase-1 (Fig. 1k) in microglial cells in the ALS motor cortex and its adjacent white matter. This was also observed in some control cases for ASC and caspase-1, and to a lesser extent for NLRP3 (Suppl. Fig. 1a–c, online resource). To further confirm that the inflammasome was expressed in microglia, we performed immunofluorescence co-staining with an antibody against Iba1 for microglia. This ensured the expression of NLRP3 (Fig. 1b–e), ASC (Fig. 1g–j), and caspase-1 (Fig. 1l–o) in microglial cells in the ALS motor cortex white and gray matter.

Next, we assessed the expression of pyroptosis effector-related proteins in the ALS motor cortex. Both cleaved GSDMD (Fig. 1p) and IL-18 (Fig. 1u) were present in ALS microglial cells, as shown by DAB immunohistochemistry. Control cases showed a few microglial cells positive for cleaved GSDMD and IL-18, but these seemed scarcer compared to ALS cases (Suppl. Fig. 1d–e, online resource). Immunofluorescence co-staining confirmed that these effector proteins were present in Iba1-positive microglial cells (Fig. 1 q–t and v–y), but not in astrocytes and oligodendrocytes, as shown by GFAP and Olig2 antibody staining respectively (Suppl. Fig. 2, online resource). Of note, antibodies against cleaved GSDMD, NLRP3, and IL-18 also faintly stained few neurons. No positive neurons were

observed for ASC and caspase-1 (Table 1). Astrocytes were rarely positive for NLRP3, caspase-1, and cleaved GSDMD, and negative for ASC and IL-18. Oligodendrocytes were negative for all inflammasome and pyroptosis effector protein markers (Table 1).

Increased presence of cleaved GSDMD-positive microglial cells in ALS precentral white matter correlates with neuronal loss

To determine whether the expression of pyroptosis-related proteins is relevant for ALS, we quantified the amount of microglia in the motor cortex positive for caspase-1 (inflammasome component) and cleaved GSDMD (pyroptosis effector). Caspase-1 was selected as inflammasome marker as this protease is responsible for the cleavage and consequent activation of downstream pyroptosis targets (i.e., GSDMD, IL-18, and IL-1β), while cleaved GSDMD was used as a marker for pyroptosis activation, as it is considered the final executor of pyroptotic cell death. In layer V of the motor cortex, we detected a decrease in the number of caspase-1-positive microglia in ALS cases compared to controls (Fig. 2a; Suppl. Table 3, online resource; $p = 0.031$; OR = 0.975; 95% CI 0.954–0.998; binary logistic regression corrected for age and sex). We did not observe any differences between ALS and control cases regarding cleaved GSDMD-positive microglia (Fig. 2b; Suppl. Table 3, online resource; $p = 0.345$; OR = 1.138; 95% CI 0.870–1.488; binary logistic regression corrected for age and sex). There was also no difference between ALS and control cases in the number of neurons in layer V of the motor cortex positive for cleaved GSDMD (Suppl. Fig. 3; Suppl. Table 3, online resource; $p = 0.527$; OR = 0.988; 95% CI 0.952–1.025; binary logistic regression corrected for age and sex) and in the precentral white matter in the number of caspase-1-positive microglial cells (Fig. 2c; Suppl. Table 3, online resource; $p = 0.4$; OR = 1.006; 95% CI 0.992–1.020; binary logistic regression corrected for age and sex). Interestingly, ALS cases showed a higher abundance of microglial cells positive for cleaved GSDMD compared to control cases in the precentral white matter (Fig. 2d; Suppl. Table 3, online resource; $p = 0.034$; OR = 1.155; 95% CI 1.011–1.319; binary logistic regression corrected for age and sex).

To examine whether the expression of pyroptosis-related proteins correlates with neuronal loss in ALS, we quantified neuronal densities in layer V of the motor cortex of ALS and control cases. Binary logistic regression corrected for age and sex showed a decrease in motor cortex layer V neuronal density in ALS compared to control cases (Fig. 3a; Suppl. Table 3, online resource; $p = 0.023$; OR = 0.880; 95% CI 0.788–0.982). Additionally, we detected a significantly higher percentage of neurons affected by pTDP-43 pathology in ALS compared to control motor cortex (Fig. 3b;

Table 1 Overview of the expression of inflammasome components and pyroptosis effector-related proteins in different cell types

	Neurons	Astrocytes	Microglia	Oligo-dendro-cytes
NLRP3	(+)	+	+++	–
ASC	–	–	+++	–
Caspase-1	–	(+)	+++	–
Cleaved GSDMD	(++)	+	+++	–
IL-18	(+)	–	+++	–

+++ abundant strongly positive cells; (+++) abundant faintly positive cells; ++ some strongly positive cells; (++) some faintly positive cells; + few strongly positive cells; (+) few faintly positive cells
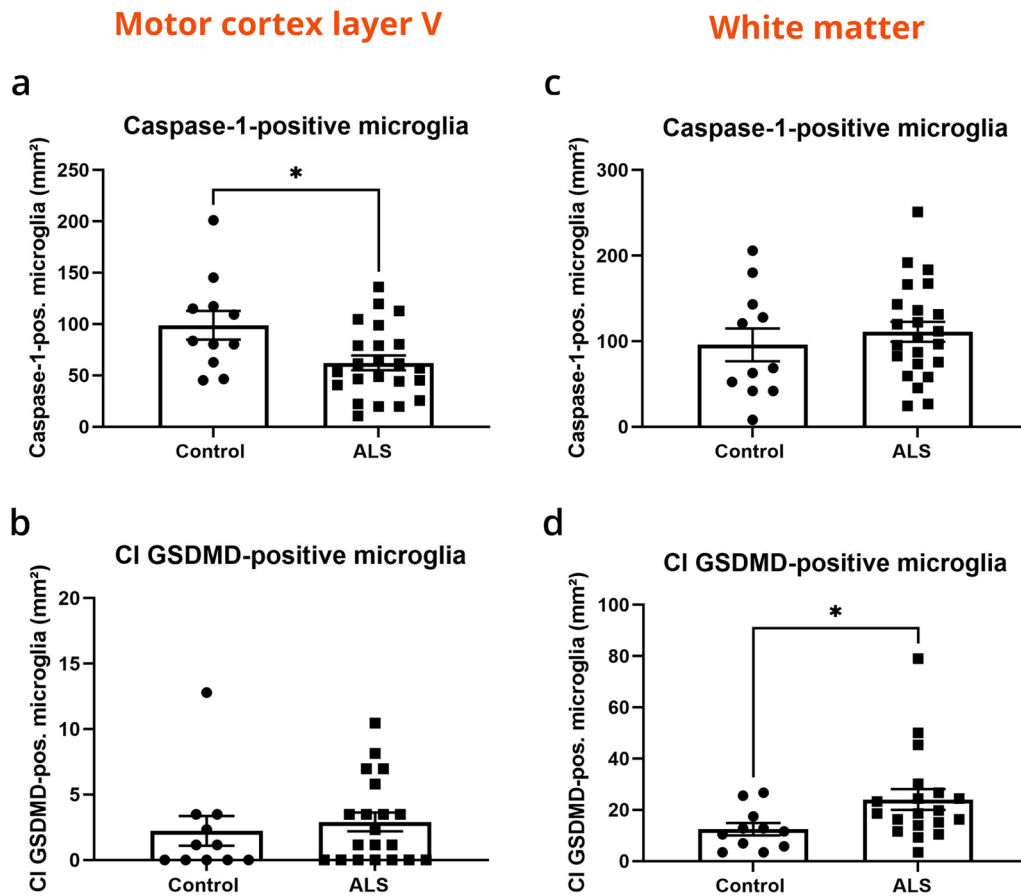
Motor cortex layer V

White matter

a

Caspase-1-positive microglia

c

Caspase-1-positive microglia

b

CI GSDMD-positive microglia

d

CI GSDMD-positive microglia

Fig. 2 Increased expression of cleaved GSDMD in ALS microglial cells in the precentral white matter. **a**, **b** Graphs representing the number of microglial cells per mm² positive for caspase-1 (**a**) and cleaved GSDMD (**b**) in layer V of the motor cortex of control and ALS cases. **c**, **d** Graphs representing the number of microglial cells per mm² positive for caspase-1 (**c**) and cleaved GSDMD (**d**) in the precentral white matter of control and ALS cases. Binary logistic regression corrected for age and sex was used for statistical analysis. *$p < 0.05$

a

Layer V neuronal density

b

% pTDP-43 affected neurons

c

TDP-43 nuclear clearance
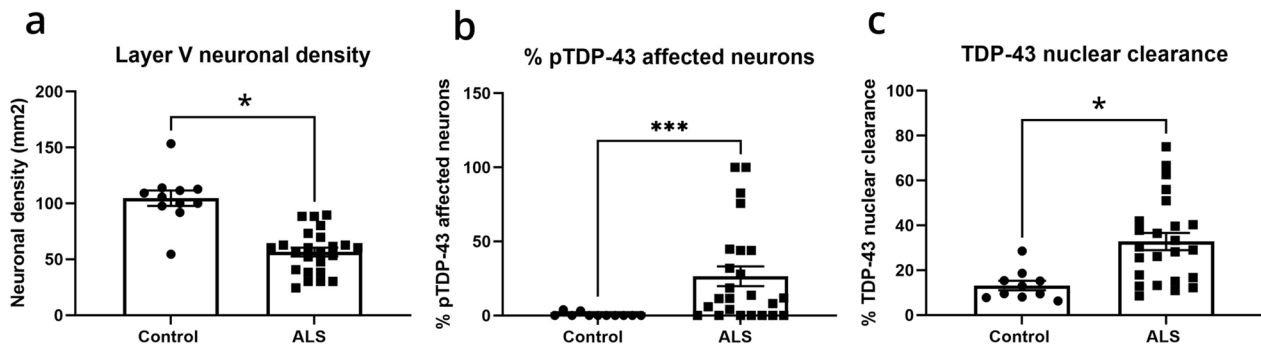
Fig. 3 Motor cortex layer V neuronal density and pTDP-43 pathology. **a** Graph representing the neuronal density per mm² in layer V of the motor cortex of control and ALS cases. **b** Graph representing the percentage of pTDP-43 affected neurons in the motor cortex of control and ALS cases. **c** Graph representing the percentage of neurons with TDP-43 cleared from the nucleus in layer V of the motor cortex. Binary logistic regression corrected for age and sex or a Mann–Whitney test was used for statistical analysis. *$p < 0.05$; ***$p < 0.001$

$p = 0.007$; Mann–Whitney test), and a significantly higher percentage of neurons with TDP-43 cleared from the nucleus in layer V of the motor cortex (Fig. 3c; Suppl. Table 3, online resource; $p = 0.022$; OR $= 1.179$; 95% CI 1.023–1.358;

binary logistic regression corrected for age and sex). A Pearson's partial correlation analysis corrected for age and sex revealed a significant correlation between the percentage of pTDP-43 affected neurons and a decreased motor cortex

Table 2 Correlation matrix for motor cortex layer V neuronal density and other parameters, corrected for age and sex

	Caspase-1 positive microglia	Cl GSDMD-positive microglia	% pTDP-43-affected neurons	Neuronal density	n
Caspase-1 positive microglia	–				25
Cl GSDMD-positive microglia	$r = 0.020; p = 0.921$	–			25
% pTDP-43 affected neurons	$r = 0.083; p = 0.682$	$r = -0.010; p = 0.960$	–		25
Neuronal density motor cortex layer V	$r = -0.343; p = 0.080$	$r = -0.431; p = 0.025$*	$r = -0.504; p = 0.007$**	–	25
% TDP-43 clearance	$r = 0.282; p = 0.163$	$r = 0.116; p = 0.572$	$r = 0.035; p = 0.865$	$r = -0.313; p = 0.119$	24

Matrix showing Pearson's correlation values and p values for the association between motor cortex layer V neuronal density and other variables, including the number of caspase-1-positive microglial cells in the precentral white matter, the number of cleaved GSDMD-positive microglial cells in the precentral white matter, the percentage of pTDP-43 affected neurons in the motor cortex, and the percentage of neurons with TDP-43 nuclear clearance in layer V of the motor cortex

*$p < 0.05$; **$p < 0.01$

layer V neuronal density (Table 2; $r = -0.504$; $p = 0.007$). Interestingly, a decreased motor cortex layer V neuronal density correlated with a higher abundance of white matter microglia positive for cleaved GSDMD (Table 2; $r = -0.431$; $p = 0.025$). In contrast, layer V neuronal density did not significantly correlate with the number of white matter microglial cells positive for caspase-1 (Table 2; $r = -0.343$; $p = 0.080$). There was also no correlation between cleaved GSDMD- and caspase-1-positive white matter microglial cells (Table 2; $r = 0.020$; $p = 0.921$). The amount of cleaved GSDMD-positive white matter microglial cells did not correlate with the percentage of pTDP-43-affected neurons (Table 2; $r = -0.010$; $p = 0.960$), nor with the percentage of neurons with TDP-43 nuclear clearance (Table 2; $r = 0.116$; $p = 0.572$). In separate linear regression models with motor cortex layer V neuronal density as dependent variable, and including age and sex as additional independent variables, the percentage of neurons affected by pTDP-43 pathology ($\beta = -0.435$; $p = 0.01$) and the number of cleaved GSDMD-positive white matter microglial cells ($\beta = -0.455$; $p = 0.021$) were good predictors of neuronal density, whereas the number of caspase-1-positive white matter microglial cells was not ($\beta = -0.244$; $p = 0.179$) (Suppl. Table 4, part 1, online resource). When combining the percentage of pTDP-43-affected neurons and cleaved GSDMD-positive white matter microglial cells in the same model, both showed to be equally potent predictors of motor cortex layer V neuronal density (Suppl. Table 4, part 2, online resource; percentage of pTDP-43-affected neurons: $\beta = -0.486$; $p = 0.004$; cleaved GSDMD-positive white matter microglial cells: $\beta = -0.464$; $p = 0.007$), indicating that they independently contribute to neuronal loss.

Elevated expression of pyroptosis-related proteins in ALS motor cortex

To further investigate the expression of pyroptosis-related proteins in ALS versus control motor cortex, we performed western blots on SDS-soluble motor cortex extracts. ALS cases showed an increased expression of the inflammasome component full-length caspase-1 (Fig. 4a, b; Suppl. Fig. 4a, online resource; $p < 0.0001$; unpaired t test) as well as the active cleaved p20 fragment (Fig. 4a, c; Suppl. Fig. 4a, online resource; $p = 0.0001$; unpaired t test). Expression of cleaved GSDMD, which represents the active cleaved fragment of GSDMD, was numerically increased in ALS cases, however not significant (Fig. 4a, d; Suppl. Fig. 4b, online resource; $p = 0.2568$; unpaired t test). Finally, the expression of the cleaved and active form of IL-18 was significantly increased in the motor cortex of ALS compared to control cases (Fig. 4a, e; Suppl. Fig. 4c, online resource; $p < 0.0001$; unpaired t test).

Presence of NLRP3 inflammasome and pyroptosis-related proteins in the ALS spinal cord does not associate with neuronal loss

Next, we assessed the presence of the inflammasome component caspase-1 and the pyroptosis effector cleaved GSDMD in the ALS spinal cord. We analyzed the amount of microglial cells positive for caspase-1 and cleaved GSDMD in the ventral and lateral white matter pyramidal tracts. There was no obvious difference between ALS and control cases in the number of caspase-1-positive microglial cells in the ventral pyramidal tracts (Fig. 5a; Suppl. Table 3, online resource; $p = 0.270$; OR = 0.947; 95% CI 0.860–1.043; binary logistic regression corrected for age and sex) and in the lateral pyramidal tracts (Fig. 5c; Suppl. Table 3, online resource;
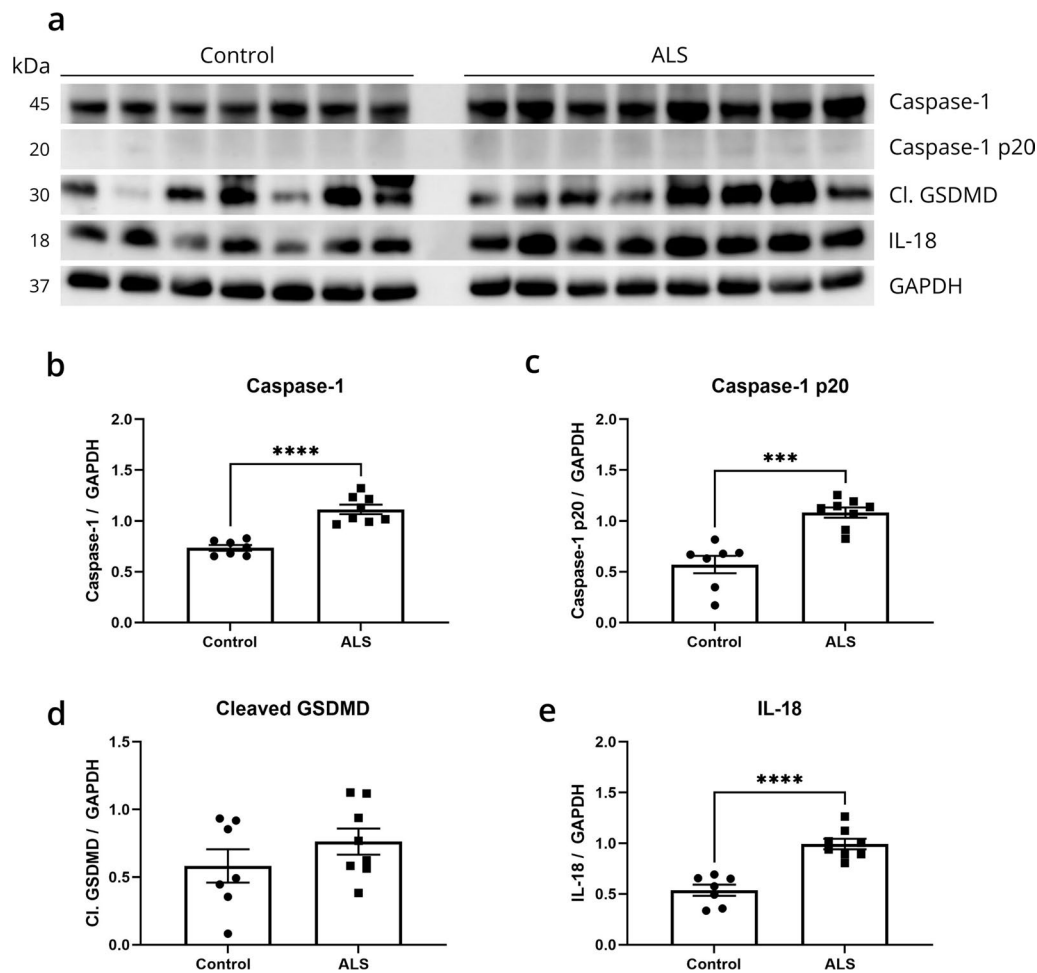
Fig. 4 Biochemical characterization of pyroptosis proteins in the ALS motor cortex. **a** Motor cortex tissue lysates from control ($n=7$) and ALS ($n=8$) on western blots probed with antibodies for caspase-1, cleaved GSDMD, and IL-18, with GAPDH as loading control. **b**–**e** Quantifications of pyroptosis-related proteins relative to GAPDH. Statistical analyses were preformed using unpaired t test. ***$p<0.001$; ****$p<0.0001$

$p=0.606$; OR $=1.002$; 95% CI 0.994–1.010; binary logistic regression corrected for age and sex). The number of cleaved GSDMD-positive microglial cells was slightly higher in ALS compared to control cases for the ventral pyramidal tracts (Fig. 5b; Suppl. Table 3, online resource; $p=0.216$; OR $=1.285$; 95% CI 0.864–1.912; binary logistic regression corrected for age and sex), and for the lateral pyramidal tracts (Fig. 5d; Suppl. Table 3, online resource; $p=0.172$; OR $=1.086$; 95% CI 0.965–1.224; binary logistic regression corrected for age and sex).

We also quantified the anterior horn neuronal density and the percentage of neurons affected by pTDP-43 pathology in the spinal cord of ALS and control cases. As expected, the anterior horn neuronal density was significantly lower in ALS compared to control cases (Suppl.

Fig. 5a; Suppl. Table 3, online resource; $p=0.017$; OR $=0.912$; 95% CI 0.846–0.984; binary logistic regression corrected for age and sex), while the percentage of pTDP-43 affected neurons was increased (Suppl. Fig. 5b, online resource, $p<0.0001$; Mann–Whitney test). A Pearson's partial correlation corrected for age and sex did not indicate any correlation between the number of cleaved GSDMD-positive microglia in the lateral pyramidal tracts and the anterior horn neuronal density (Suppl. Table 5, online resource; $r=0.045$; $p=0.832$), nor with the percentage of pTDP-43-affected neurons (Suppl. Table 4, online resource; $r=0.208$; $p=0.318$). However, the anterior horn neuronal density correlated with the percentage of neurons affected by pTDP-43 pathology, similar to our
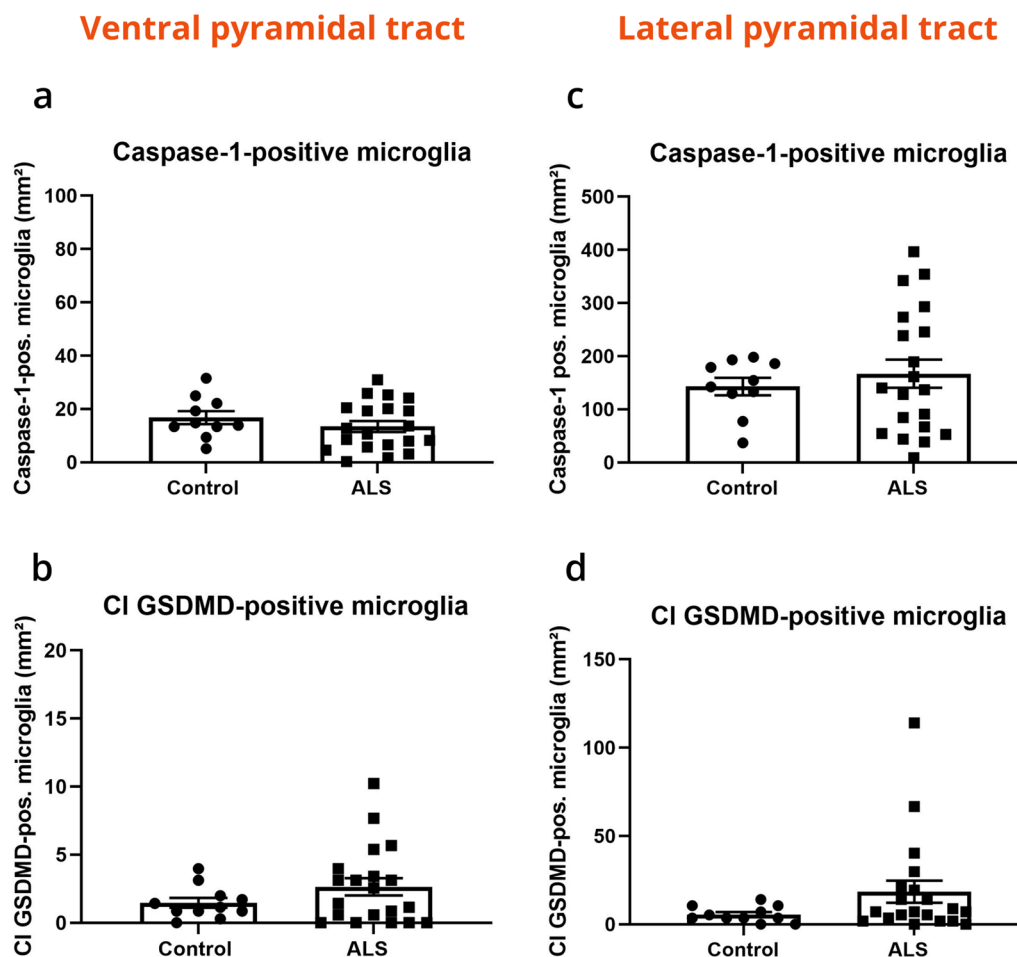
Ventral pyramidal tract

Lateral pyramidal tract

Fig. 5 Expression of caspase-1 and cleaved GSDMD in ALS and control spinal cord pyramidal tract microglia. **a**, **b** Graphs representing the number of microglial cells per mm² positive for caspase-1 (**a**) and cleaved GSDMD (**b**) in the ventral pyramidal tracts of control and ALS spinal cord. **c**, **d** Graphs representing the number of microglial cells per mm² positive for caspase-1 (**c**) and cleaved GSDMD (**d**) in the lateral pyramidal tracts of control and ALS spinal cord. Binary logistic regression corrected for age and sex was used for statistical analysis

observations in the motor cortex (Suppl. Table 5, online resource; $r = -0.544$; $p = 0.004$).

Finally, we biochemically assessed the expression of pyroptosis-related proteins in the spinal cord of ALS and control cases. ALS SDS-soluble spinal cord extracts displayed an increased expression of full-length caspase-1 (Fig. 6a, b; Suppl. Fig. 6a, online resource; $p = 0.0134$; unpaired t test), as well as the cleaved and active p20 fragment (Fig. 6a, c; Suppl. Fig. 6a, online resource; $p = 0.0002$; unpaired t test). Additionally, we detected an increased expression of pyroptosis effector proteins cleaved GSDMD (Fig. 6a, d; Suppl. Fig. 6b, online resource; $p = 0.0003$; unpaired t test) and IL-18 (Fig. 6a, e; Suppl. Fig. 6c, online resource; $p = 0.0022$; Mann–Whitney test).

Increased GSDMD reactivity in symptomatic TDP-43^A315T transgenic mice is associated with a decreased neuronal density in the brain

To explore whether the pyroptosis pathway was also activated in animal models of ALS, we investigated the presence of the inflammasome component caspase-1 and the pyroptosis effector protein GSDMD in the brain and spinal cord of TDP-43^A315T transgenic mice. We detected microglia positive for caspase-1 (Fig. 7a; Suppl. Fig. 7a–d, online resource) and GSDMD (Fig. 7b; Suppl. Fig. 7e–h, online resource) in the gray and white matter of the motor cortex and spinal cord of symptomatic TDP-43^A315T transgenic mice. We quantified the number of caspase-1- and GSDMD-positive microglial cells per mm² in the motor cortex and in the spinal cord (gray + white matter) in five different mouse groups: (1) 6 month old wild-type mice, (2) 16 month old wild-type mice, (3) 6 month old TDP-43^A315T transgenic
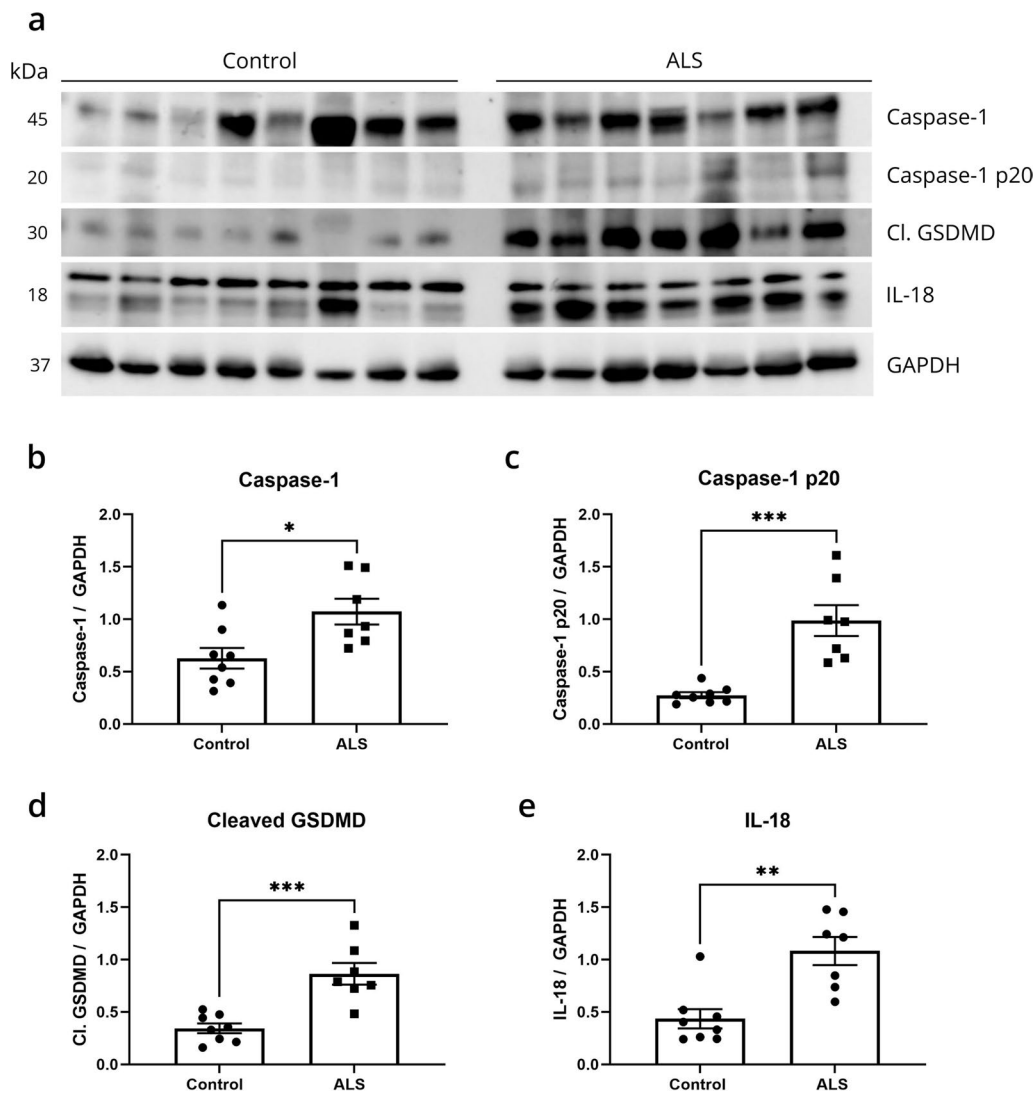
Fig. 6 Biochemical characterization of pyroptosis proteins in the ALS spinal cord. **a** Spinal cord tissue lysates from control ($n = 8$) and ALS ($n = 7$) on western blots probed with antibodies for caspase-1, cleaved GSDMD, and IL-18, with GAPDH as loading control. For IL-18, the lower band is the correct molecular weight, as the upper band represents pro-IL-18. **b–e** Quantifications of pyroptosis-related proteins relative to GAPDH. Statistical analyses were performed using unpaired t test or Mann–Whitney test. *$p < 0.05$; **$p < 0.01$; ***$p < 0.001$

mice, (4) 16 month old TDP-43[A315T] transgenic mice, and (5) symptomatic TDP-43[A315T] transgenic mice (6–14 months old, mean age of 9 months). In the motor cortex, the number of caspase-1-positive microglia was significantly increased in 16 month old wild-type and 16 month old TDP-43[A315T] transgenic mice compared to their 6 month old counterparts (Fig. 7c; wild-type: $p = 0.0289$; TDP-43[A315T] transgenic: $p = 0.0149$; one-way ANOVA followed by Tukey's multiple comparisons). The number of caspase-1-positive microglial cells was not increased in the brain of symptomatic TDP-43[A315T] transgenic mice. In contrast, the amount of GSDMD-positive microglial cells was significantly increased in symptomatic TDP-43[A315T] transgenic compared

to 6 month old wild-type mice (Fig. 7d; $p = 0.0014$; one-way ANOVA followed by Tukey's multiple comparisons), 16 month old wild-type mice ($p = 0.0039$); 6 month old TDP-43[A315T] transgenic mice ($p = 0.0006$) and 16 month old TDP-43[A315T] transgenic mice ($p = 0.0041$). In the spinal cord, a similar increase in caspase-1-positive microglia was detected as in the brain in 16 month old wild-type and TDP-43[A315T] transgenic mice, although not significant (Fig. 7e). Symptomatic TDP-43[A315T] transgenic mice showed similar levels of caspase-1-positive microglial cells in the spinal cord compared to the 16 month old groups. Finally, we analyzed the amount of GSDMD-positive microglial cells in the spinal cord. Similar to as was observed in the brain, this was
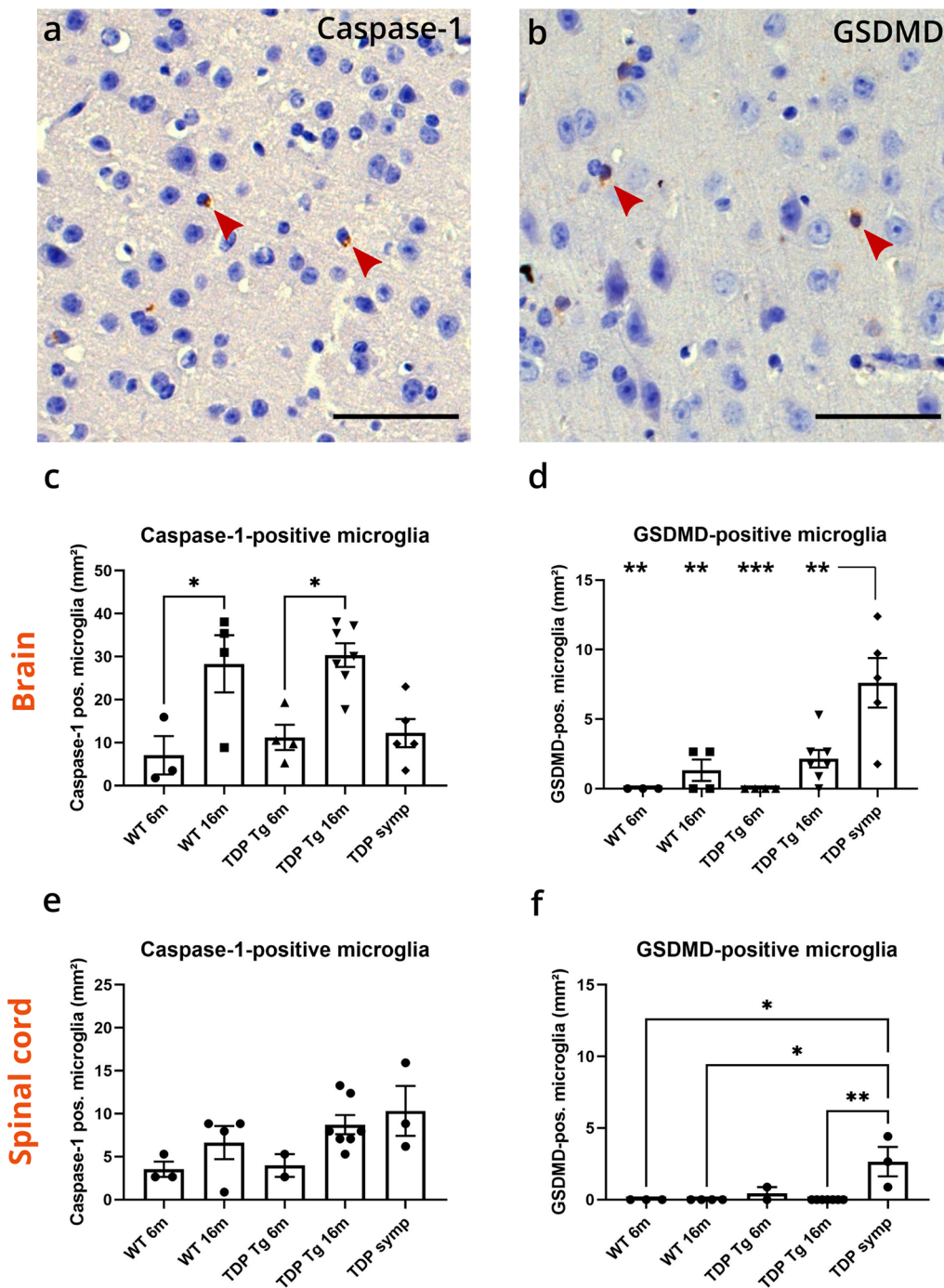
Fig. 7 Increased expression of GSDMD in motor cortex and spinal cord of symptomatic TDP-43[A315T] transgenic mice. **a** Immunohistochemical representative image of caspase-1-positive microglia (arrowheads) in the motor cortex of TDP-43[A315T] transgenic mice. **b** Immunohistochemical representative image of GSDMD-positive microglia (arrowheads) in the motor cortex of TDP-43[A315T] transgenic mice. Scale bars represent 50 µm. **c, d** Graphs representing the number of caspase-1 (**c**) and GSDMD (**d**) positive microglial cells per mm² in the motor cortex of the different mouse groups. **e, f** Graphs representing the number of caspase-1 (**e**) and GSDMD (**f**) positive microglial cells per mm² in the spinal cord of the different mouse groups. WT 6 m = 6-month-old wild-type mice; WT 16 m = 16-month-old wild-type mice; TDP Tg 6 m = 6-month-old TDP-43[A315T] transgenic mice; TDP Tg 16 m = 16-month-old TDP-43[A315T] transgenic mice; TDP symp = symptomatic TDP[A315T] transgenic mice. *$p < 0.05$; **$p < 0.01$; ***$p < 0.001$

significantly increased in symptomatic TDP-43[A315T] transgenic mice compared to 6 month old wild-type mice (Fig. 7f; $p = 0.0267$; Kruskal–Wallis test followed by Dunn's multiple comparisons), 16 month old wild-type mice ($p = 0.0133$), and 16 month old TDP-43[A315T] transgenic mice ($p = 0.0038$).

Next, we focused on TDP-43, as this protein is mutated in the mouse model. No typical cytoplasmic TDP-43-positive inclusions were observed, although symptomatic TDP-43[A315T] transgenic mice occasionally displayed dense aggregated material around the nucleus positive for TDP-43 (Suppl. Fig. 8a, online resource; arrow), while the nucleus was not stained. Nuclear clearance of physiological TDP-43 was a prominent phenotype, which we quantified for the different mouse groups. In the motor cortex, TDP-43 nuclear clearance was significantly increased in symptomatic TDP-43[A315T] transgenic mice compared to 16 month old wild-type mice (Suppl. Fig. 8a, c, online resource; $p = 0.006$; Kruskal–Wallis test followed by Dunn's multiple comparisons). We also noticed a numerical but non-significant increase in the 16 month old TDP-43[A315T] transgenic group. In the spinal cord anterior horn, no differences in TDP-43 nuclear clearance could be detected among the groups (Suppl. Fig. 8b, d, online resource).

We further analyzed the different mouse groups immunohistochemically using an antibody against ubiquitin, as it was previously shown that ubiquitin-positive but TDP-43-negative material could be detected in this model [48]. We observed diffuse cytoplasmic ubiquitin-positive staining in neurons both in the motor cortex (Suppl. Fig. 9a, online resource) and in the spinal cord (Suppl. Fig. 9b, online resource) of the majority of symptomatic TDP-43[A315T] transgenic mice. This ubiquitin-positive neuronal staining was also observed in one 6-month-old and two 16-month-old TDP-43[A315T] transgenic asymptomatic mice. An antibody against SQSTM1/p62 displayed a similar neuronal staining pattern, for the first time indicating that affected neurons in symptomatic TDP-43[A315T] transgenic mice are positive for SQSTM1/p62 (Suppl. Fig. 9c, d, online resource). Finally, we assessed the neuronal density in layer V of the motor cortex and the anterior horn of the spinal cord of the different mouse groups to evaluate whether neuronal loss was present in the model. Neuronal density was significantly decreased in the motor cortex of symptomatic TDP-43[A315T] transgenic mice compared to 6-month-old wild-type mice (Suppl. Fig. 10a, online resource; $p = 0.0307$; Kruskal–Wallis test followed by Dunn's multiple comparisons). In the spinal cord, a slight but non-significant decrease was observed in the symptomatic TDP-43[A315T] transgenic mice (Suppl. Fig. 10b, online resource).

Using Pearson's partial correlation analysis, we found that the number of GSDMD-positive microglial cells in the brain significantly correlated with a decrease in motor cortex layer V neuronal density (Table 3; $r = -0.478$; $p = 0.021$). This was not the case for caspase-1-positive microglia (Table 3; $r = -0.378$; $p = 0.075$). The percentage of TDP-43 nuclear clearance also correlated with layer V neuronal density (Table 3; $r = -0.414$; $p = 0.049$). There was also a trend towards a correlation between the amount of GSDMD-positive microglia and the percentage of TDP-43 nuclear clearance, although not significant (Table 3; $r = 0.408$; $p = 0.053$). A similar analysis for the spinal cord did not show any significant correlations for the above-mentioned parameters (Suppl. Table 6, online resource).

Discussion

Here, we described the expression of the NLRP3 inflammasome complex comprising of NLPR3, ASC, and caspase-1, as well as pyroptosis effector-related proteins cleaved GSDMD and IL-18 in microglial cells in the ALS motor cortex and spinal cord. The microglial expression of cleaved GSDMD in the precentral white matter correlated with neuronal loss in layer V of the motor cortex, but not with the amount of pTDP-43 pathology. In the spinal cord, no increase in microglial cleaved GSDMD was detected, although elevated expression of pyroptosis-related proteins was detected biochemically both in the motor cortex and in the spinal cord (Table 4). Importantly, we observed increased GSDMD expression in microglia in the brain and

Table 3 Correlation matrix for mouse motor cortex neuronal density and other parameters

	Caspase-1-positive microglia	GSDMD-positive microglia	% TDP-43 clearance	n
Caspase-1-positive microglia	–			23
GSDMD-positive microglia	$r = -0.075$; $p = 0.733$	–		23
% TDP-43 clearance	$r = -0.168$; $p = 0.442$	$r = 0.408$; $p = 0.053$	–	23
Layer V neuronal density	$r = -0.378$; $p = 0.075$	$r = -0.478$; $p = 0.021$*	$r = -0.414$; $p = 0.049$*	23

Matrix showing Pearson's correlation values and p values for the association between mouse motor cortex layer V neuronal density and other variables, including the number of caspase-1-positive microglial cells, the number of GSDMD-positive microglial cells, and the percentage of TDP-43 nuclear clearance

*$p < 0.05$; **$p < 0.01$

Table 4 Overview for the comparison of IHC versus WB results for caspase-1 and cleaved GSDMD in the human and mouse motor cortex and spinal cord

CASPASE-1		IHC	WB
Human ALS	Motor cortex	WM = GM ↓	Pro-caspase-1 ↑ Caspase-1 p20 ↑
	Spinal cord	WM =	Pro-caspase-1 ↑ Caspase-1 p20 ↑
Mouse TDP-43 A315T	Motor cortex	=	
	Spinal cord	=	
CLEAVED GSDMD		**IHC**	**WB**
Human ALS	Motor cortex	WM ↑ GM =	cl GSDMD ↗
	Spinal cord	WM ↗	cl GSDMD ↑
Mouse TDP-43 A315T	Motor cortex	↑	
	Spinal cord	↑	

In immunohistochemical stainings, the number of cells expressing a given protein was assessed, whereas by western blot, the general expression levels were determined

GM gray matter; *WM* white matter; *IHC* immunohistochemistry; *WB* western blot; ↑ significant increase; ↗ numerical trend towards increase; "=" no noticeable difference; ↓ significant decrease

spinal cord of symptomatic TDP-43^{A315T} transgenic mice, which also correlated with neuronal loss in layer V of the motor cortex, similar to our observations in human tissue. To our knowledge, this is the first time that expression of the full NLRP3 inflammasome and, importantly, the pyroptosis effector-related proteins cleaved GSDMD and IL-18 was observed in ALS microglial cells and was linked to neuronal degeneration, both in human *post-mortem* tissue and TDP-43 transgenic mice.

In human ALS brain, we observed a correlation of the abundance of pTDP-43 pathology with neuronal loss, but not with cleaved GSDMD-positive white matter microglia, although the latter lesions are also associated with motor cortex neuron loss. This suggests that the presence of pTDP-43 aggregates does not directly influence the activation of pyroptosis in white matter microglia. However, this is an end-point observation, and it is possible that during the course of the disease, pathological pTDP-43, soluble or aggregated, does serve as a trigger for inflammasome and pyroptosis activation. Evidence supports the activation of the NLRP3 inflammasome by abnormal protein aggregates in neurodegenerative diseases [19, 52]. This activation requires a two-step process. First, the NFκB pathway is activated through stimulation of Toll-like receptors (TLRs), leading to upregulation of the expression of NLRP3, pro-caspase-1, and pro-interleukins. Second, the NLRP3 inflammasome can be assembled and activated by a variety of stimuli, such as reactive oxygen species (ROS), extracellular ATP, lysosomal rupture, low intracellular K$^+$, and aggregated or misfolded proteins [15, 39, 54]. Regarding ALS, in vitro studies showed that pathological TDP-43 could induce an NLRP3-dependent secretion of active IL-1β and IL-18 in microglia [10, 25, 53]. This pro-inflammatory cascade was shown to be toxic to motor neurons, while in the absence of microglia, pathological TDP-43 was not detrimental to motor neurons [53]. Similar results were obtained with mutant SOD1, which was shown to trigger the NLRP3-dependent cleavage of caspase-1 and IL-1β in primary mouse microglia [10]. These results support the hypothesis that pathological ALS proteins can induce pyroptosis activation in microglia. In recent years, several groups also demonstrated an upregulation of NLRP3, ASC, caspase-1, IL-1β, and IL-18 in SOD1^{G93A} mice and rats [2, 8, 10, 16, 22, 29], which are the most commonly used animal models for ALS, although SOD1 mutations only explain 2% of ALS cases [43]. Deora and colleagues also showed increased expression of the NLRP3 inflammasome in TDP^{Q331K} mutant mice [10]. Furthermore, TDP-43 was shown to interact with NFκB and to function as a suppressor of the NFκB pathway, with a loss of TDP-43 leading to increased activation of the NFκB pathway [55]. This suggests that a loss of nuclear TDP-43, as observed in ALS, could make cells more susceptible for pyroptosis activation through a reduced inhibition of the NFκB pathway. Although the above data indicate the importance of pathological TDP-43 and SOD1 in eliciting pyroptosis activation, it is likely that other pathological conditions often observed in ALS (e.g., ROS and extracellular ATP), which could be downstream of SOD1 and TDP-43 mutations, are responsible for NLRP3 inflammasome activation.

In human ALS cases, the abundance of cleaved GSDMD-positive microglia in the precentral white matter correlated

with a decreased neuronal density in layer V of the motor cortex. Following pyroptosis activation, GSDMD-NT oligomerizes and associates with the plasma membrane to form micropores, resulting in potassium efflux, intracellular and extracellular ion imbalance, cell swelling, and rupture of the plasma membrane [39]. This causes massive leakage of pro-inflammatory cytokines, such as IL-1β and IL-18, as well as other cytosolic components [15, 50]. In turn, IL-1β and IL-18 bind their respective receptors on glial cells and neurons, initiating a complex spectrum of signaling pathways, further enhancing inflammatory responses and resulting in neuronal injury and death [39]. Therefore, it is likely that the observed activation of the pyroptosis pathway in ALS white matter microglia contributes to neuronal degeneration in the motor cortex, possibly by affecting axonal health. However, it remains unclear whether this is the primary insult in neurodegeneration, or just one contributing factor enhancing neuronal toxicity among others. Importantly, the number of microglial cells in the human white matter is significantly higher compared to gray matter [26]. Furthermore, a clear difference in the immune regulatory profile was identified between white and gray matter microglia, with white matter microglia displaying an increased expression of genes involved in the NFκB pathway [44]. This could make white matter microglia more susceptible for pyroptosis activation as activation of the NFκB pathway induces elevated expression of pyroptosis-related genes, possibly explaining the increased abundance of cleaved GSDMD-positive microglia specifically in the ALS precentral white matter.

We did not observe obvious TDP-43 pathological aggregates in the brain and spinal cord of symptomatic TDP-43^{A315T} mice, although a few ubiquitin-positive neurons were detected in symptomatic TDP-43^{A315T} mice, and to a lesser extent in 6 and 16 month old TDP-43^{A315T} mice. This is in line with previous reports [18, 20, 48]. In the motor cortex of symptomatic TDP-43^{A315T} mice, we detected an increased TDP-43 nuclear clearance. This did not significantly correlate with the amount of GSDMD-positive microglia, similar to our observations in the human brain. Importantly, a decrease in neuronal density in layer V of the motor cortex correlated with an increased presence of GSDMD-positive microglia, mirroring our human data. Others also detected a decreased number of neurons in layer V of the motor cortex [48, 51]. In the spinal cord, results are more contradictory with some groups reporting up to 20% loss of spinal motor neurons [11, 48], while we and others could not confirm this [20]. This could be due to the small number of mice from which we could obtain spinal cord tissue, which is one of the limitations of this study.

In human cases, we detected an average of 32.8% neurons cleared of nuclear TDP-43 in ALS cases using an antibody directed against the C-terminal part of TDP-43, with control cases showing an average of 13.18% neurons negative

for nuclear TDP-43. Our human control cohort showed relatively high basal levels of TDP-43 nuclear depletion, especially when compared to 6- and 16-month-old wild-type mice. Since previous studies [28, 33] described this phenomenon, but, to our knowledge, did not provide quantitative data, it is unclear whether the detection of TDP-43 nuclear clearance in control cases is a physiological finding, or whether it is due to technical reasons (antibody sensitivity in formalin-fixed tissue) or autolysis during the *post-mortem* interval. Importantly, it was shown that cellular stress can induce the depletion of TDP-43 from the nucleus [38], which also occurs in normal aging and during the agonal phase before death, possibly explaining the relatively high baseline levels of TDP-43 nuclear clearance in the human control cohort. In contrast, mice were euthanized under anesthesia and brains were immediately harvested, resulting in less cellular stress and therefore possibly lower levels of baseline TDP-43 nuclear clearance. More studies on TDP-43 nuclear clearance including other TDP-43 antibodies will be needed to clarify its biology.

Contrary to cleaved GSDMD, we did not observe an increase of caspase-1-positive microglial cells in ALS versus control precentral gray and white matter using immunohistochemical methods (Table 4). It is likely that mainly physiological inactive pro-caspase-1 is detected by immunohistochemistry, which might mask the detection of increased levels of the active p20 fragment as observed by western blot (Table 4). It seems that full-length pro-caspase-1 is endogenously present in microglia, as control cases also show basal caspase-1 levels. Furthermore, the abundance of caspase-1-positive microglia is fivefold higher compared to cleaved GSDMD-positive microglia in human cases, indicating a physiological expression of pro-caspase-1 in microglia. Using biochemical methods, we, however, observed an increased expression of both pro-caspase-1 as well as the p20 active fragment in human ALS brain and spinal cord (Table 4), probably reflecting a higher cellular expression without an increase in the number of caspase-1 expressing microglial cells. Therefore, it is likely that in ALS microglial cells upscale their expression of pro-caspase-1, and that following NLRP3 inflammasome activation the p20 fragment is produced, as reflected by our western blot data (Table 4). We detected similar results in mice, as symptomatic TDP-43^{A315T} did not show an increase in caspase-1-positive microglia. However, an age-dependent effect was noted as 16-month-old wild-type and TDP-43^{A315T} transgenic mice presented with a higher abundance of caspase-1-positive microglia compared to their 6-month-old counterparts. This age-dependent increase of caspase-1 expression was recently described in mice and humans and referred to as 'inflammaging', reflecting the increased expression of inflammatory proteins during the aging process [30]. Additionally, the *post-mortem* interval and other comorbid neurological and

agonal conditions may influence the inflammatory status in the human brain and spinal cord, likely explaining the higher baseline levels of caspase-1 and cleaved GSDMD-positive microglial cells in human *post-mortem* tissue compared to wild-type and TDP-43[A315T] transgenic mice, where these parameters are better controlled. A limitation of this study is that we could not assess caspase-1 full length and p20 fragment levels biochemically by western blot in mouse brain and spinal cord due to unavailability of frozen tissue.

Our biochemical analysis in CNS lysates showed an increased expression of active IL-18 in ALS motor cortex and spinal cord compared to control cases, indicative of an activated pyroptosis pathway. Elevated serum IL-18 levels have previously also been demonstrated in sporadic ALS patients [21]. Other groups reported elevated caspase-1, NLRP3, and IL-18 levels in ALS brain tissue [22, 23], which is in line with our results for caspase-1, p20, and IL-18 in the motor cortex and spinal cord. Increased NLRP3 mRNA levels were also detected in blood and in *post-mortem* tissue of ALS patients [1, 32]. Unfortunately, antibodies against NLRP3 and IL-1β could not detect the respective proteins in *post-mortem* brain and spinal cord lysates by western blot in our hands, which is a limitation of this study. Regarding the active fragment of GSDMD, we showed for the first time an increased expression of cleaved GSDMD in ALS versus control cases, which was significant in the spinal cord. It is possible that in the motor cortex, baseline expression of cleaved GSDMD in neurons in both control and ALS cases, as observed by IHC, masks the increased cleaved GSDMD expression in microglial cells on western blot.

In the CNS, PRRs are thought to mainly be expressed by microglial cells and astrocytes [50]. Both cell types also are assumed to be able to express NLRP3; however, for neurons, this is still debated [39]. In this study, we observed expression of the full NLRP3 inflammasome (i.e., NLRP3, ASC, and caspase-1) as well as the pyroptosis effector-related proteins cleaved GSDMD and IL-18 in microglia. NLRP3 and cleaved GSDMD expression were additionally detected in neurons and astrocytes, although to a lesser extent. ASC was exclusively detected in microglia, while caspase-1 was also occasionally faintly stained in astrocytes. IL-18 was absent in astrocytes, with some neurons faintly positive. Oligodendrocytes were negative for all above-mentioned markers. Our results underline the importance of microglia in inflammasome-mediated pyroptosis in ALS, and are in line with several in vitro studies, showing that microglia express the full NLRP3 inflammasome and produce active IL-1β and IL-18 [10, 25, 53]. Bellezza and colleagues also demonstrated expression of the NLRP3 inflammasome in SOD1[G93A] mouse microglial cells [2], although others found increased microglial caspase-1 and ASC expression

in the same mouse model, but not NLRP3 [29]. In contrast, another group postulated mainly astrocytes, but also neurons to express ASC and NLRP3, with microglia only positive for ASC in SOD1[G93A] mice [8, 22]. A recent study, however, detected NLRP3 expression both in microglia and astrocytes of SOD1[G93A] mice [10], similar to our results in the human ALS brain. Overall, evidence points towards microglia as the main cell type responsible for pyroptosis activation in ALS, although we cannot fully exclude that astrocytes and possibly neurons also contribute to NLRP3 inflammasome-mediated cytotoxicity.

In conclusion, our findings point towards microglial NLRP3 inflammasome-mediated pyroptosis as an important player in ALS pathophysiology and neurodegeneration, with cleaved GSDMD as a useful marker for pyroptosis activation in the ALS precentral white matter. Investigation of the pathological triggers and the effects of inhibition of this pathway in vitro and in vivo will aid in the development of novel therapeutic strategies counteracting motor neuron degeneration in ALS.

Author contributions EVS: study design and coordination, immunohistochemistry, immunofluorescence, protein extraction, western blotting, microscopic assessments, neuropathology, statistical analysis, and manuscript drafting and preparation. SO: mouse immunohistochemistry, immunofluorescence, and critical review of the manuscript. SM: immunohistochemistry, western blotting, and critical review of the manuscript. ST: design of mouse study, mouse genotyping, and critical review of the manuscript. AR: design of mouse study, mouse breeding, mouse sacrificing and tissue collection, and critical review of the manuscript. OO: human immunohistochemistry, western blotting, and critical review of the manuscript. JW and ACL: clinical neurology and critical review of the manuscript. PVD: clinical neurology, study design, and critical review of the manuscript. LVDB: study design and critical review of the manuscript. DRT: study design and supervision, neuropathology, and manuscript preparation. All authors read and approved the final manuscript.

Declarations

References

1. Banerjee P, Elliott E, Rifai OM, O'Shaughnessy J, McDade K, Abrahams S et al (2022) NLRP3 inflammasome as a key molecular target underlying cognitive resilience in amyotrophic lateral sclerosis. J Pathol 256:262–268. https://doi.org/10.1002/path.5846
2. Bellezza I, Grottelli S, Costanzi E, Scarpelli P, Pigna E, Morozzi G et al (2018) Peroxynitrite activates the NLRP3 inflammasome cascade in SOD1(G93A) mouse model of amyotrophic lateral sclerosis. Mol Neurobiol 55:2350–2361. https://doi.org/10.1007/s12035-017-0502-x
3. Braak H, Alafuzoff I, Arzberger T, Kretzschmar H, Del Tredici K (2006) Staging of Alzheimer disease-associated neurofibrillary pathology using paraffin sections and immunocytochemistry. Acta Neuropathol 112:389–404. https://doi.org/10.1007/s00401-006-0127-z
4. Brooks BR, Miller RG, Swash M, Munsat TL (2000) El Escorial revisited: revised criteria for the diagnosis of amyotrophic lateral sclerosis. Amyotroph Lateral Scler Other Motor Neuron Disord 1:293–299. https://doi.org/10.1080/146608200300079536
5. de Carvalho M, Dengler R, Eisen A, England JD, Kaji R, Kimura J et al (2008) Electrodiagnostic criteria for diagnosis of ALS. Clin Neurophysiol 119:497–503. https://doi.org/10.1016/j.clinph.2007.09.143
6. De Carvalho M, Swash M (2009) Awaji diagnostic algorithm increases sensitivity of El Escorial criteria for ALS diagnosis. Amyotroph Lateral Scler 10:53–57. https://doi.org/10.1080/17482960802521126
7. Debray S, Race V, Crabbé V, Herdewyn S, Matthijs G, Goris A et al (2013) Frequency of C9Orf72 repeat expansions in amyotrophic lateral sclerosis: a Belgian cohort study. Neurobiol Aging 34:2890.e7-2890.e12. https://doi.org/10.1016/j.neurobiolaging.2013.06.009
8. Debye B, Schmülling L, Zhou L, Rune G, Beyer C, Johann S (2018) Neurodegeneration and NLRP3 inflammasome expression in the anterior thalamus of SOD1(G93A) ALS mice. Brain Pathol 28:14–27. https://doi.org/10.1111/bpa.12467
9. Denes A, Brough D (2012) Caspase-1: is IL-1 just the tip of the ICEberg? Cell Death Dis 3:e338. https://doi.org/10.1038/cddis.2012.86
10. Deora V, Lee JD, Albornoz EA, Mcalary L, Jagaraj CJ, Robertson AAB et al (2019) The microglial NLRP3 inflammasome is activated by amyotrophic lateral sclerosis proteins. Glia 68:407–421. https://doi.org/10.1002/glia.23728
11. Espejo-Porras F, Piscitelli F, Verde R, Ramos JA, Di Marzo V, de Lago E et al (2015) Changes in the endocannabinoid signaling system in CNS structures of TDP-43 transgenic mice: relevance for a neuroprotective therapy in TDP-43-related disorders. J Neuroimmune Pharmacol 10:233–244. https://doi.org/10.1007/s11481-015-9602-4
12. Frank D, Vince JE (2019) Pyroptosis versus necroptosis: similarities, differences, and crosstalk. Cell Death Differ 26:99–114. https://doi.org/10.1038/s41418-018-0212-6
13. Gao J, Wang L, Huntley ML, Perry G, Wang X (2018) Pathomechanisms of TDP-43 in neurodegeneration. J Neurochem 146:7–20. https://doi.org/10.1111/jnc.14327
14. Gorno-Tempini ML, Hillis AE, Weintraub S, Kertesz A, Mendez M, Cappa SF et al (2011) Classification of primary progressive aphasia and its variants. Neurology 76:1006–1014. https://doi.org/10.1212/WNL.0b013e31821103e6
15. Guan Y, Han F (2020) Key mechanisms and potential targets of the NLRP3 inflammasome in neurodegenerative diseases. Front Integr Neurosci 14:37. https://doi.org/10.3389/fnint.2020.00037
16. Gugliandolo A, Giacoppo S, Bramanti P, Mazzon E (2018) NLRP3 inflammasome activation in a transgenic amyotrophic lateral sclerosis model. Inflammation 41:93–103. https://doi.org/10.1007/s10753-017-0667-5
17. Hardiman O, Al-Chalabi A, Chio A, Corr EM, Logroscino G, Robberecht W et al (2017) Amyotrophic lateral sclerosis. Nat Rev Dis Prim 3:17071. https://doi.org/10.1038/nrdp.2017.71
18. Hatzipetros T, Bogdanik LP, Tassinari VR, Kidd JD, Moreno AJ, Davis C et al (2014) C57BL/6J congenic Prp-TDP43A315T mice develop progressive neurodegeneration in the myenteric plexus of the colon without exhibiting key features of ALS. Brain Res 1584:59–72. https://doi.org/10.1016/j.brainres.2013.10.013
19. Heneka MT, Kummer MP, Stutz A, Delekate A, Saecker A, Griep A et al (2013) NRLP3 is activated in Alzheimer's disease and contributes to pathology in APP/PS1 mice. Nature 493:674–678. https://doi.org/10.1038/nature11729.NLRP3
20. Herdewyn S, Cirillo C, Van Den Bosch L, Robberecht W, Vanden Berghe P, Van Damme P (2014) Prevention of intestinal obstruction reveals progressive neurodegeneration in mutant TDP-43 (A315T) mice. Mol Neurodegener 9:24. https://doi.org/10.1186/1750-1326-9-24
21. Italiani P, Carlesi C, Giungato P, Puxeddu I, Borroni B, Bossù P et al (2014) Evaluating the levels of interleukin-1 family cytokines in sporadic amyotrophic lateral sclerosis. J Neuroinflammation 11:94. https://doi.org/10.1186/1742-2094-11-94
22. Johann S, Heitzer M, Kanagaratnam M, Goswami A, Rizo T, Weis J et al (2015) NLRP3 inflammasome is expressed by astrocytes

in the SOD1 mouse model of ALS and in human sporadic ALS patients. Glia 63:2260–2273. https://doi.org/10.1002/glia.22891

23. Kadhim H, Deltenre P, Martin JJ, Sébire G (2016) In-situ expression of Interleukin-18 and associated mediators in the human brain of sALS patients: Hypothesis for a role for immune-inflammatory mechanisms. Med Hypotheses 86:14–17. https://doi.org/10.1016/j.mehy.2015.11.022

24. Koper MJ, Van Schoor E, Ospitalieri S, Vandenberghe R, Vandenbulcke M, Von Arnim CAF et al (2019) Necrosome complex detected in granulovacuolar degeneration is associated with neuronal loss in Alzheimer's disease. Acta Neuropathol 139:463–484. https://doi.org/10.1007/s00401-019-02103-y

25. Leal-lasarte M, Franco JM, Labrador-garrido A, Pozo D (2017) Extracellular TDP-43 aggregates target MAPK/MAK/MRK overlapping kinase (MOK) and trigger caspase-3 / IL-18 signaling in microglia. FASEB 7:2797–2816. https://doi.org/10.1096/fj.201601163R

26. Lee J, Hamanaka G, Lo EH, Arai K (2019) Heterogeneity of microglia and their differential roles in white matter pathology. CNS Neurosci Ther 25:1290–1298. https://doi.org/10.1111/cns.13266

27. Lee J, Hyeon SJ, Im H, Ryu H, Kim Y, Ryu H (2016) Astrocytes and microglia as non-cell autonomous players in the pathogenesis of ALS. Exp Neurobiol 25:233. https://doi.org/10.5607/en.2016.25.5.233

28. Mackenzie IRA, Bigio EH, Ince PG, Geser F, Neumann M, Cairns NJ et al (2007) Pathological TDP-43 distinguishes sporadic amyotrophic lateral sclerosis from amyotrophic lateral sclerosis with SOD1 mutations. Ann Neurol 61:427–434. https://doi.org/10.1002/ana.21147

29. Meissner F, Molawi K, Zychlinsky A (2010) Mutant superoxide dismutase 1-induced IL-1beta accelerates ALS pathogenesis. Proc Natl Acad Sci 107:13046–13050. https://doi.org/10.1073/pnas.1002396107

30. Mejias NH, Martinez CC, Stephens ME, De Rivero Vaccari JP (2018) Contribution of the inflammasome to inflammaging. J Inflamm 15:23. https://doi.org/10.1186/s12950-018-0198-3

31. Mirra SS, Heyman A, McKeel DW, Sumi SM, Crain BJ, Brownlee LM et al (1991) The Consortium to Establish a Registry for Alzheimer's Disease (CERAD): II. Standardization of the neuropathologic assessment of Alzheimer's disease. Neurology 41:479–486

32. Moreno-García L, Miana-Mena FJ, Moreno-Martínez L, de la Torre M, Lunetta C, Tarlarini C et al (2021) Inflammasome in ALS skeletal muscle: NLRP3 as a potential biomarker. Int J Mol Sci 22:2523. https://doi.org/10.3390/ijms22052523

33. Neumann M, Sampathu DM, Kwong LK, Truax AC, Micsenyi MC, Chou TT et al (2006) Ubiquitinated TDP-43 in frontotemporal lobar degeneration and amyotrophic lateral sclerosis. Science (80) 314:130–133. https://doi.org/10.1126/science.1134108

34. Philips T, Robberecht W (2011) Neuroinflammation in amyotrophic lateral sclerosis: role of glial activation in motor neuron disease. Lancet Neurol 10:253–263

35. Rascovsky K, Hodges JR, Knopman D, Mendez MF, Kramer JH, Neuhaus J et al (2011) Sensitivity of revised diagnostic criteria for the behavioural variant of frontotemporal dementia. Brain 134:2456–2477. https://doi.org/10.1093/brain/awr179

36. Renton AE, Chio A, Traynor BJ (2014) State of play in amyotrophic lateral sclerosis. Nat Neurosci 17:17–23. https://doi.org/10.1038/nn.3584

37. Rosenbohm A, Peter RS, Erhardt S, Lulé D, Rothenbacher D, Ludolph AC et al (2017) Epidemiology of amyotrophic lateral sclerosis in Southern Germany. J Neurol 264:749–757. https://doi.org/10.1007/s00415-017-8413-3

38. Scotter EL, Chen HJ, Shaw CE (2015) TDP-43 proteinopathy and ALS: insights into disease mechanisms and therapeutic targets. Neurotherapeutics 12:352–363. https://doi.org/10.1007/s13311-015-0338-x

39. Song L, Pei L, Yao S, Wu Y, Shang Y (2017) NLRP3 inflammasome in neurological diseases, from functions to therapies. Front Cell Neurosci 11:63. https://doi.org/10.3389/fncel.2017.00063

40. Swinnen B, Robberecht W (2014) The phenotypic variability of amyotrophic lateral sclerosis. Nat Rev Neurol 10:661–670. https://doi.org/10.1038/nrneurol.2014.184

41. Taylor JP, Brown RH, Cleveland DW (2016) Decoding ALS: from genes to mechanism. Nature 539:197–206. https://doi.org/10.1126/science.1249098

42. Thal DR, Rüb U, Schultz C, Sassin I, Ghebremedhin E, Del Tredici K et al (2000) Sequence of Aβ-protein deposition in the human medial temporal lobe. J Neuropathol Exp Neurol 59:733–748. https://doi.org/10.1093/jnen/59.8.733

43. Van Damme P, Robberecht W, Van Den Bosch L (2017) Modelling amyotrophic lateral sclerosis: progress and possibilities. Dis Model Mech 10:537–549. https://doi.org/10.1242/dmm.029058

44. Van der Poel M, Ulas T, Mizee MR, Hsiao C, Miedema SSM, Schuurman KG et al (2019) Transcriptional profiling of human microglia reveals grey-white matter heterogeneity and multiple sclerosis-associated changes. Nat Commun 10:1139. https://doi.org/10.1038/s41467-019-08976-7

45. Van Schoor E, Koper MJ, Ospitalieri S, Dedeene L, Tomé SO, Vandenberghe R et al (2020) Necrosome-positive granulovacuolar degeneration is associated with TDP-43 pathological lesions in the hippocampus of ALS/FTLD cases. Neuropathol Appl Neurobiol 47:328–345. https://doi.org/10.1111/nan.12668

46. Vande Walle L, Lamkanfi M (2016) Pyroptosis. Curr Biol 26:R568–R572. https://doi.org/10.1016/j.cub.2016.02.019

47. Wang X, Chi J, Huang D, Ding L, Zhao X, Jiang L et al (2020) α-synuclein promotes progression of Parkinson's disease by upregulating autophagy signaling pathway to activate NLRP3 inflammasome. Exp Ther Med 19:931–938. https://doi.org/10.3892/etm.2019.8297

48. Wegorzewska I, Bell S, Cairns NJ, Miller TM, Baloh RH (2009) TDP-43 mutant transgenic mice develop features of ALS and frontotemporal lobar degeneration. PNAS 106:18809–18814. https://doi.org/10.1073/pnas.0908767106

49. Wijesekera LC, Leigh PN (2009) Amyotrophic lateral sclerosis. Orphanet J Rare Dis 4:3. https://doi.org/10.1186/1750-1172-4-3

50. Xie Z, Zhao G (2014) Pyroptosis and neurological diseases. Neuroimmunol Neuroinflammation 1:60–65. https://doi.org/10.4103/2347-8659.139716

51. Zhang W, Zhang L, Liang B, Schroeder D, Zhang Z, Cox GA et al (2016) Hyperactive somatostatin interneurons contribute to excitotoxicity in neurodegenerative disorders. Nat Neurosci 19:557–559. https://doi.org/10.1038/nn.4257

52. Zhang X, Wang R, Hu D, Sun X, Fujioka H, Lundberg K et al (2020) Oligodendroglial glycolytic stress triggers inflammasome activation and neuropathology in Alzheimer's disease. Sci Adv 6:eabb8680. https://doi.org/10.1126/sciadv.abb8680

53. Zhao W, Beers DR, Bell S, Wang J, Wen S, Baloh RH et al (2015) TDP-43 activates microglia through NF-κB and NLRP3 inflammasome. Exp Neurol 273:24–35. https://doi.org/10.1016/j.expneurol.2015.07.019

54. Zhou K, Shi L, Wang Y, Chen S, Zhang J (2016) Recent advances of the NLRP3 inflammasome in central nervous system disorders. J Immunol Res 2016:9238290. https://doi.org/10.1155/2016/9238290

55. Zhu J, Cynader MS, Jia W (2015) TDP-43 inhibits NF-κB activity by blocking p65 nuclear translocation. PLoS ONE 10:e0142296. https://doi.org/10.1371/journal.pone.0142296